



Photocatalytic cement composite surface reactivation impact on the degradation rate of methylene blue in a circulating flow fixed-bed photoreactor

Sama Tajasosi^a, Ramazan Vagheei^{a,*}, Mehdi Shirzad-Siboni^{b,c}

^aDepartment of Water and Environmental Engineering, Faculty of Civil Engineering, Shahrood University of Technology, Shahrood, Iran, Tel. +989154293887; email: rvagheei@gmail.com/rvagheei@shahroodut.ac.ir (R. Vagheei), Tel. +989369064452; email: sama.tajasosi@yahoo.com (S. Tajasosi)

^bResearch Center of Health and Environment, Guilan University of Medical Sciences, Rasht, Iran

^cDepartment of Environmental Health Engineering, School of Health, Guilan University of Medical Sciences, Rasht, Iran, Tel. +989112346428; email: mshirzadsiboni@yahoo.com

Received 17 May 2022; Accepted 23 September 2022

ABSTRACT

The use of polymers or ceramics as a fixed-bed in photoreactors, other than causing complexities and environmental pollution, imposes high costs on treatment systems. This study used photocatalytic cement composite as a practical and economic material for a bed. To evaluate the impact of cement matrix characteristics on the photocatalytic activity of the bed surface, six different mix designs with two water binder ratio of 0.28 and 0.42 was considered. Furthermore, 0%, 5% and 10% of cement content was replaced by silica fume. In addition, the effect of acid treatment on increasing the degradation rate of methylene blue was investigated. Standard tests were performed to determine the mechanical properties of the composites, and spectroscopic tests were carried out to evaluate the changes in methylene blue concentration on the extracted samples. In addition, improving the mechanical properties of the composite did not lead to a significant decrease in the performance of photocatalytic treatment. Due to their higher abrasion resistance, high-performance composites are considered efficient materials in terms of durability and pollution. The microstructural evaluation also proved the role of acid treatment in increasing the contact surface and TiO₂ particles' appearance on the composite surface.

Keywords: Photoreactor; Methylene blue; Photocatalytic degradation; TiO₂; Cement composite

1. Introduction

Titanium dioxide (TiO₂) is a widely used semiconductor material in various industries for various photocatalytic processes, producing heterogeneous catalysts, solar cells, gas sensors and corrosion protection [1, 2]. The performance of TiO₂ particles in the degradation of organic materials, especially in the presence of H₂O molecules, is a topic that has received attention in recent studies [3]. However, the use of TiO₂ as a powder (free particles) in gas and water treatment has some serious challenges, including limited

effective surface area, poor gas diffusion and light transmission blockage requires energy-consuming separation processes such as ultrafiltration to reuse and prevent diffusion in the treated water [4–6]. This matter increases the complexity of the process and the operating cost and is one of the main obstacles to commercialization. Stabilizing TiO₂ particles on solid substrates such as alumina, silica, iron oxide, biopolymers, and cementitious composites such as concrete provides an opportunity to overcome this challenge [7]. The hardened cement matrix is mainly composed of amorphous calcium silicate hydrate (CSH) structures due to the hydration of Ca₃SiO₅ and Ca₂SiO₄ crystals

* Corresponding author.

[8]. Based on their research, CSH gel consists of two morphological types: internal CSH, as hydration chains in the boundary areas of cement particles and outer CSH, which exists inside the open space between the cement particles and in the water that surrounds them. Another hydration product that precipitates widely between cement grains is crystalline calcium hydroxide (Portlandite). These two products of cement particle hydration determine how the cement matrix works on a large scale [9]. Nanoscale modifications of cementitious composites have also been widely considered to increase the performance of cementitious materials [10–12]. Nowadays, various materials are used as photocatalytic substrates. Concrete is a promising photocatalytic bed candidate due to its low cost, wide-range production, and durability. Therefore, it has a good potential for developing small to large-scale water treatment systems. Furthermore, TiO_2 , as one of the most widely used photocatalytic materials, has a good research background [13, 14]. Adding TiO_2 to cement paste increases the rate of cement hydration [15, 16]. One of the first applications of TiO_2 as a photocatalyst in the construction industry is self-cleaning products. These elements, typically made with white Portland cement-based self-cleaning composite technology, are suitable for building facades [17]. Despite proven functional properties, the technical aspects of the photocatalytic application of these composites in the construction industry still have limitations in the case of pollution treatment using natural sunlight [18]. Relatively high band gaps of TiO_2 , the electron–hole recombination time and the inactivation of TiO_2 by intermediate blocks occupying catalytically active sites are among the limitations of these particles working with the visible light spectrum [19]. Studies have emphasized the importance of amorphous TiO_2 microstructures for achieving optimal photocatalytic activity through interaction with surrounding ions [20] or silica-based media [21]. These environments can change the active spectral band of TiO_2 and the rate of hydration of cementitious products. Hydrated amorphous matrices have a more significant spatial distance than the size of anatase TiO_2 particles and can support Ti^{3+} species under UV irradiation close to their surface. This phenomenon can explain the photocatalytic performance of TiO_2 particles on the surface of cementitious composites [22]. The utilization of fixed-bed reactors to perform chemical processes and, in the case of this branch of research, the treatment of water pollutants, has made significant progress, and different geometries and methods for the design and development of these reactors in various stages of research and industry can be found [23]. Furthermore, comprehensive research in the engineering and modeling of photocatalytic reactors has been done, and the results related to the industrial potential of such reactors have been well formulated in scientific documents [24]. The development of continuous flow reactors for photocatalytic purification of fluids has always been a growing research area, mainly coating methods for layering TiO_2 particles on the inner wall of these reactors are the focusing subject of this research. The sol–gel method is considered one of the most common techniques for preparing TiO_2 -coated surfaces for photocatalytic purification [25]. The use of photocatalytic cement composites in the removal of air pollutants is also one of

the topics pursued by researchers, although the studies on these composites in the water treatment field are still limited and unknown [26]. Extensive research has been conducted on the degradation of dyes such as methylene blue using a variety of photocatalysts [27–29]. Furthermore, dye degradation over photocatalytic substrates has a relatively good research background [30, 31]. The application of quartz labyrinth as a photocatalytic fixed-bed is one of the studies used to degrade dyes such as Acid Red 18. Under very low water flow rates, significant treatment efficiencies have been reported [32]. Various studies have considered photocatalytic cementitious composites for degrading dye contaminants. The treatment of color-polluted wastewater has been studied using different commercial cement products containing TiO_2 [33,34]. Fixed-bed tubular reactors, particularly due to their relatively simple structure and suitable contact surface under UV irradiation, have a unique appeal for photocatalytic degradation of dyes. One of the first specialized studies in this field, which also focused on methylene blue, belonged to Ling et al. [27]. They used industrial TiO_2 (anatase) in their study. The results of the experiments showed that the performance of the tubular photoreactor was very similar to that of TiO_2 powder-based slurry reactors. This research domain has also applied newer UV light sources to degrade dyes such as methylene blue in tubular reactors. UV LED lamps, in particular, have shown successful performance [35]. More specialized research can be found in the degradation of organic dyes based on solid substrates coated with TiO_2 , including the study of Sá et al. [46]. They used micro-reactor systems and meager fluid flow rates and reported much higher degradation efficiencies than meso-reactor systems. Practical engineering and implementation of photocatalytic cement composites for water treatment require a comprehensive understanding of how several interrelated parameters affect the performance of the composite and the continuous reactivity of the surface of these composites. These parameters, which are still under investigation, include cementitious compounds, hardened cement matrix microstructure, and characteristics of TiO_2 particles. Evaluating the impact of these features and their interaction requires complex experiment programs. The objective of this study was to understand the effects of additives and their properties on the performance of photocatalytic cement composites based on a set of the control parameter to remove the methylene blue (MB) pollutant from water and then evaluate and analyze the obtained results based on the composition of the composites and their interaction with TiO_2 used in photocatalytic degradation of MB as a pollutant.

In this study, unlike other research, nanomaterials were not used in a pure or doped form, and industrial TiO_2 was used in the photocatalytic cement composite structure. Nanoparticles (due to carcinogenicity) and polymer coatings (due to the production of microplastics followed by erosion), whose dangers for the environment have been scientifically proven, were not used. Also, for the first time on a laboratory scale, a relatively high initial volume (up to 5 L of water contaminated with MB) and a macroscale reactor were used for testing in order to significantly reduce measurement errors. Energy consumption has been significantly

reduced using LED technology, and ordinary reactivation techniques, including acid treatment processes, are among the novelties of this research.

2. Materials and methods

2.1. Materials

In the present study, methylene blue (MB) was purchased from Alvan Sabet Co., (Hamadan, Iran). Chemical structure and summary of MB properties is presented in Table 1. White Portland cement from Urmia White Cement Co., (Urmia, Iran), and silica fume from Iran Ferrosilice Co. with chemical characteristics reported in Table 2 were used to fabricate photocatalytic cement composite (PCC) pipes. The white Portland cement specifications were in accordance with the ASTM C150 [36] standard. Silica fume compatible with

Table 1
Chemical structure and characteristics of methylene blue

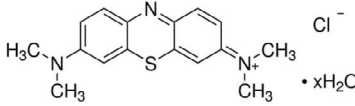
Structure	
Formula	$C_{16}H_{18}ClN_3S \cdot xH_2O$
Density (g/mL at 20°C)	1.0
λ_{max} (nm)	664
M_w (g/mol)	319.85
Solubility in water (g/L)	43.6

Table 2
Chemical compositions of cement and silica fume (provided by the manufacturer)

Compound	Cement (%)	Silica fume (%)
CaO	66.5	1.87
SiO ₂	23.18	89.22
Al ₂ O ₃	4.528	1.2
Fe ₂ O ₃	0.392	2.12
MgO	0.77 ± 0.1	1.61
K ₂ O	0.12	1.056
Na ₂ O	0.35	0.556
L.O.I.	2.39 ± 0.5	2.6
Total	-98.23	100.232

Table 3
Mix designs of photocatalytic cementitious composites

Mix code	Cement (kg/m ³)	Silica fume (kg/m ³)	TiO ₂ (kg/m ³)	Water + superplasticizer (kg/m ³)	Aggregate (kg/m ³)
P10	810	0	90	342	987
P10S5	765	45	90	342	996
P10S10	720	90	90	342	1,005
HP10	810	0	90	225	1,325
HP10S5	765	45	90	225	1,308
HP10S10	720	90	90	225	1,317

the standard specifications of ASTM C1240 [37] was used in mixed proportions as a partial replacement for cement. Silica sand from Parsilis Co., (Hamadan, Iran) passing sieve No. 30 (smaller than 600 μm) was used as aggregate. FARCOPLAST P100-3R polycarboxylate-based superplasticizer from Shimi Sakhteman Co., (Tehran, Iran), with a specific gravity of 1.1 g/cm³ was used as a high-range water-reducing agent. This superplasticizer is compatible with the standard specifications of ASTM C494 [38] type G. Industrial anatase TiO₂ (COSMO Chemical Co., KA-100, Ulsan, Korea) with an average particle diameter of 300 nm, minimum purity of 98% (provided by the manufacturer) and specific gravity of 3.96 g/cm³ was used in mix proportions.

2.2. Fabrication of specimens

According to Table 3, the amount of cement replacement with silica fume in the mix designs is 0, 5 and 10 wt.% of the total cement content. For every 5% of silica fume, 45 kg/m³ of the amount of cement is reduced, and the same amount of silica fume is added to the mixture. The sum of water and superplasticizer to powder materials (sum of cement, silica fume and TiO₂) is a fixed value of 0.38 for the P series in mix designs. In the code of each design that includes the letter S, the percentage of silica fume used is mentioned. The presence of the letter H in the design code means higher mechanical properties, which originates from the lower ratio of the sum of water and superplasticizer to powder materials (0.25). The amount of TiO₂ based on the preliminary tests carried out to obtain the maximum photocatalytic performance and maintain the desired mechanical characteristics was considered 10% by weight of the powder material and equivalent to 90 kg/m³.

Fabricating, molding and curing of standard specimens were performed in accordance with the requirements of the ASTM C109 [39] test method. The PCC tube was made with the specified mold to achieve the required dimensions. Firstly, cementitious materials, including cement and silica fume (if applicable), were mixed for about 1 min to gain a homogenous mixture of dry materials. Then the silica sand was added, and mixing was continued for another 2 min. TiO₂ was added gradually to the dry mix, and the mixing process continued at a high speed of 72 rpm. The blend of water and superplasticizer was added at the end, and the mixing rate was slowed down to 30 rpm for about 1 min until the paste was formed. Finally, for another 60 s, mixing was performed at the high-speed procedure. The water-to-cementitious material ratio was selected differently in two mix designs to achieve normal (N) and

high-performance (HP) cement composites. Due to the use of different ratios of powder materials, superplasticizer content was considered in different weight percentages to obtain mixtures with desirable workability. The specimens were demolded after 24 h and immersed in a water tank until the testing date (28 d). Table 3 shows the mixed proportion designs of this study.

2.3. Acid treatment process

To treat the surface of photocatalytic cement composite parts with hydrochloric acid, these parts are placed in a container containing 4 L of 2.5 M hydrochloric acid solution at a temperature of $20^{\circ}\text{C} \pm 3^{\circ}\text{C}$ for 3 min. Then after washing with tap water and a plastic brush to remove loose surface particles, they were placed in a container containing tap water for 2 h. Then the surface of the parts was washed again with water and a brush and placed in the reactor for the test.

2.4. Experimental setup

A photocatalytic reactor with the following specifications was constructed to measure the performance of specimens. The UV irradiation system was installed on the axis of the cylindrical reactor. The photocatalytic cement composite pipe was placed inside the reactor tube, a photocatalytic fixed-bed. The inner wall of the pipe, with an average diameter of 50 mm and a limited length of 230 mm (total surface area of 361.1 cm^2), was irradiated with a set of UV LEDs having a total power of 24 W and a narrow wavelength of 395 nm. This UV source provided the irradiated power of 66.5 mW/cm^2 . Initial concentrations of 4, 8 and 12 mg/L were selected for MB polluted water. The upper limit of concentration was selected based on the capacity of the reactor and the power of the lamp. The next two concentrations were considered in order to compare the effect of concentration on the level of surface reaction in the early times and also its effect on the change in degradation rate; the effect of concentration on performance in the mentioned period was one of the other considerations for choosing these three concentrations. The proximity of the initial concentration values is due to the possibility of comparing the effect of concentration on the continuity of the degradation rate. In other words, the end of the time range of one concentration could be used as a reference tool at the beginning of the time range of another concentration. In this manner, the possibility of measuring surface saturation is provided. A total water volume of 5 L in the main tank with a temperature of 25°C and approximate pH of 7 was guided through the reactor using a utility pump with a constant flow rate of 12 L/min. The additional pH measures were tested on a specific specimen (P10S5) to ensure the reactor performance in various alkali/acid environments. Water circulation inside the reactor continued for 4 h. The arrangement in Fig. 1 shows a schematic view of the built-in treatment system. Fig. 2 shows a PCC pipe specimen, and Fig. 3 shows the reactor body, which is made of stainless steel, and the screw cap at the end of the body allows the specimen to be replaced. Sampling was conducted during the treatment and from the main tank at 30-min intervals.

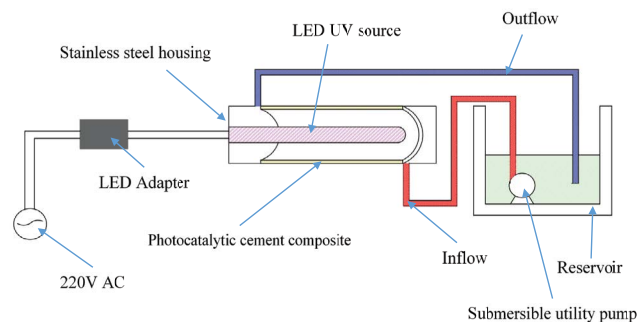


Fig. 1. Schematic diagram of laboratory arrangement of photocatalytic treatment system based on PCC fixed-bed photoreactor.



Fig. 2. Thin-walled tube specimen made of PCC.

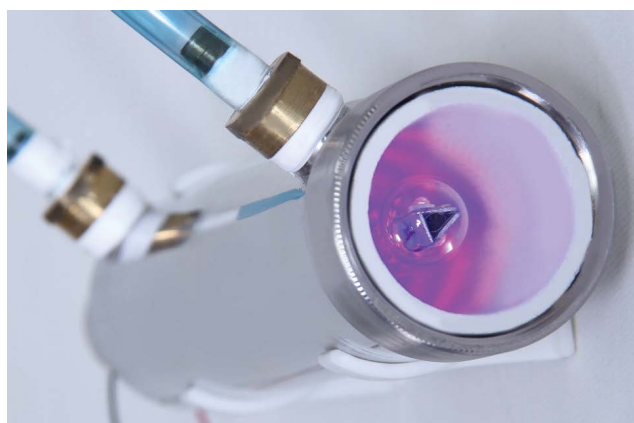


Fig. 3. Front view of the reactor body and the position of tube and lamp inside it.

2.5. Standard tests

The compressive strength test was performed based on the ASTM C109 test method. The compressive strength of the cubic specimens with the dimension of 50 mm was measured at 28 d to compare the role of cementitious materials and evaluate the contribution of TiO_2 to the results. The flexural strength tests were performed based on the notations of the ASTM C348 [40] test method. Prismatic

specimens with the dimensions of 40 mm × 40 mm × 160 mm were fabricated and subjected to three-point flexural loading. The abrasion resistance test was performed based on the ASTM C944 [41] test method. Since the standard states that the specimens can be in any shape and size, the specimens with the dimensions of 100 mm × 100 mm × 20 mm were fabricated so that the abrasion device could accommodate the specimens. After removing the specimen from the water tank at 28 d, they were air-dried, and a cloth cleaned the surface; then, the test was implemented in 32-min periods. After determining the initial mass of a specimen, it was fastened in the abrasion device, and the rotating cutter was mounted on the surface of the specimen. After every 2 min, the surface of the specimen was cleaned with a brush, and weight loss was measured with a scale contributing 0.1 g accuracy. The test was carried out on three different specimens to gain an average of the mass loss of a specific mix design, and the results were reported by weight loss percentage for the total 6 min of abrasion.

Methylene blue concentration was measured by UV-Vis spectroscopy with a wavelength of 664 nm, and the calibration curve was determined. In this project, 324 spectroscopic experiments were performed on water samples contaminated with methylene blue. Due to the extensively large volume of the initial polluted water (5,000 mL) and the relatively low power of the UV source, the MB concentration decrease is almost linear. So the degradation rate can be calculated using the slope function of MB concentrations in excel software on the data collection for each specimen under each set of controlled parameters during the 4-h test period.

3. Results and discussion

3.1. Mechanical properties

Cement composites based on TiO₂ industrial photocatalyst, which were designed and manufactured in two categories: N and HP, in terms of compressive strength, were tested at the age of 28 d, and their mechanical properties, as shown in Table 3, were reported. Based on the presented results, adding silica fume has improved mechanical properties in both strength classes, so in the normal category, up to 11.7%, and in the high-performance category, up to 20.8%, an increase in compressive strength was observed. This improvement in strength is essential in fixed-bed reactors because reducing erosion and increasing the durability of the composite surface exposed to water flow, which may also contain suspended solid contaminants, fewer contaminants enter the water from the composite surface, and the durability of the bed is increased substantially. Accordingly, the abrasion resistance test, which directly represents the surface durability of composites against erosion, has also been performed, and a meaningful relationship between the results is conceivable. A 45.2% abrasion loss reduction (ALR) by adding 10% silica fume to the mix design in the normal category and a 50% reduction in the high-performance category shows the positive effect of silica fume. On the other hand, a significant decrease of 64.5% abrasion loss with increasing the strength class and the simultaneous effect of silica fume compared to the base design indicates

the high potential of these composites in performance under severe conditions.

3.2. Scanning electron microscopy and energy-dispersive X-ray analysis

A well-hydrated cement matrix shows significant resistance to corrosive agents such as acids if it loses its structural alkalinity due to the pozzolanic reaction and a dense CSH structure surrounding TiO₂ particles. However, to what extent is this resistance sufficient to provide effective porosity on the surface after acid treatment to increase the level of photocatalytic contact? This question, which can be seen visually in Fig. 4, illustrates the optimized specimen with the highest degradation rate. The microstructure of the surface of P10S5 shown in Fig. 4 shows a considerably high surface porosity due to acid treatment at a magnification of 135kx. In this scale, cavities with dimensions less than 200 nm are noticeable, which, according to energy-dispersive X-ray (EDS) analysis, are created between TiO₂ particles. In other words, a strong cement matrix has surrounded TiO₂ particles due to a pozzolanic reaction. These particles are preserved, and the weaker bonds and impurities are removed due to the reaction with acid. This process creates a highly active and, at the same time, abrasion-resistant contact surface, which provides the photocatalytic capability of TiO₂ particles on the specimen surface in this specified fixed-bed photoreactor. The EDS analysis implied in Figs. 5 and 6 shows the presence of TiO₂ particles on the surface and depth of the specimen. The high concentration of particles on the surface of the specimen, which is caused by acid treatment, is observable in Fig. 6. This could be the reason for the high efficiency of the P10S5 specimen.

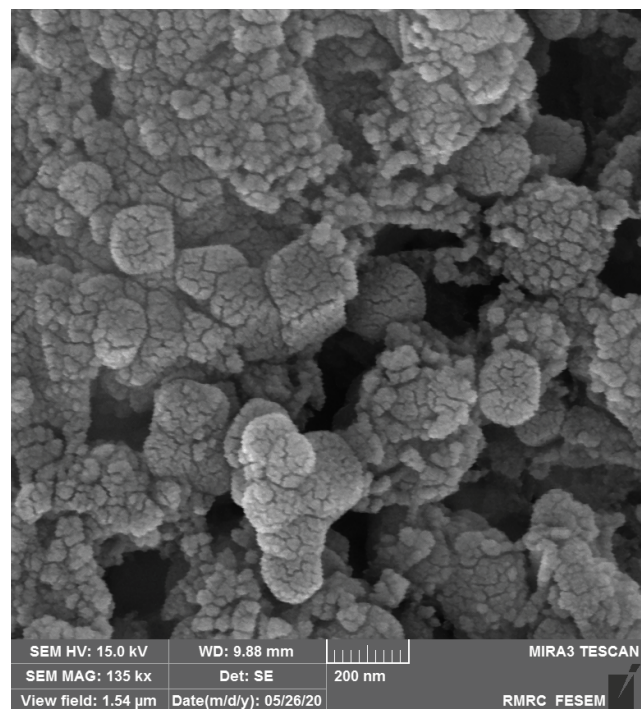


Fig. 4. Microstructure of P10S5 PCC surface after acid treatment.

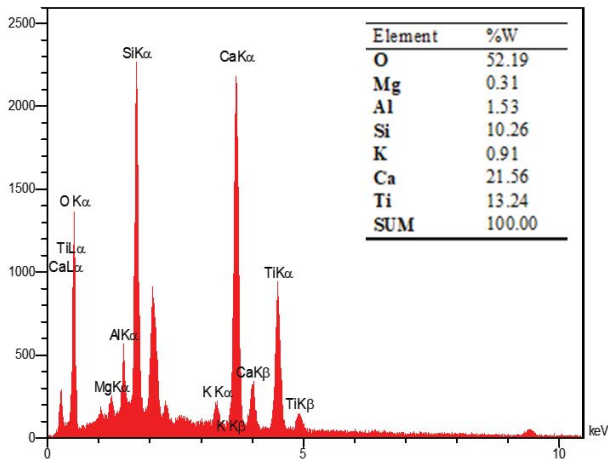


Fig. 5. General EDS results of PCC P10S5 and the percentage of detected elements.

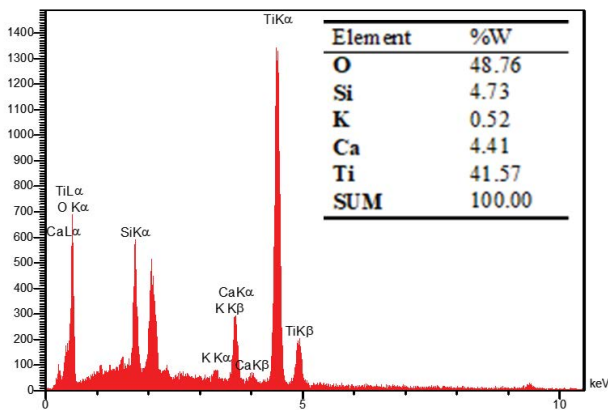


Fig. 6. Surface EDS analysis of PCC P10S5 and the percentage of detected elements.

3.3. Effects of operational parameters on the photocatalytic removal of MB

The degradation rates shown in Figs. 7–9, obtained for different concentrations of methylene blue contaminant, are based on the results of 30-min tests over 4 h period and the calculation of the slope of the fitting curve between the results. Fig. 7 shows the results of experiments on the water with the lowest initial MB concentration and shows two sets of data related to composite pipes before and after acid treatment. Based on the fitted results, the maximum methylene blue degradation rate of 0.327 mg/h belongs to the HP10S5 specimen. This rate, which is 7.9% higher than the P10 specimen degradation rate, can be attributed to the effect of the dense matrix and the positive role of silica fume on the performance of TiO₂ particles. However, this trend has decreased in the higher percentage of silica fume in the case of the HP10S10 specimen, which is probably because excess amounts of silica fume particles surround TiO₂ particles. The acid treatment process has a positive effect on the performance of all pipes, and from 14.4% to 36.6% increase in degradation rate has been achieved.

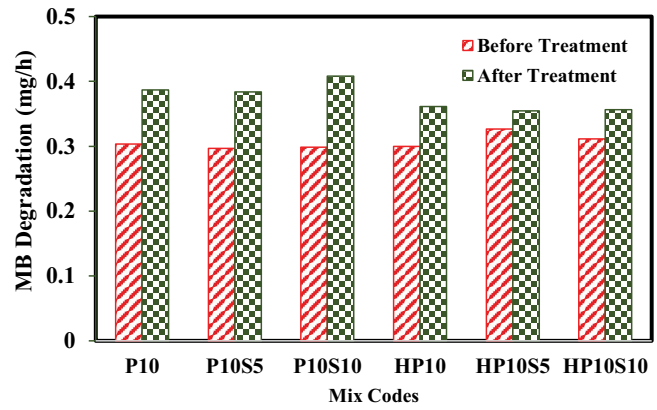


Fig. 7. Degradation rate of methylene blue before and after acid treatment ($Q = 12$ L/min, $pH = 7$, $C_0 = 4$ mg/L, $T = 25^\circ C$).

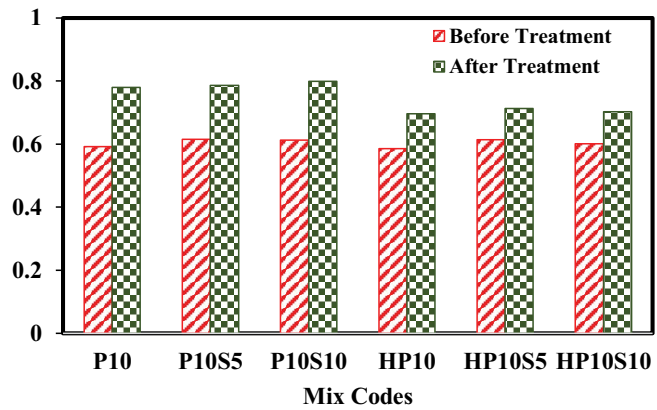


Fig. 8. Degradation rate of methylene blue before and after acid treatment ($Q = 12$ L/min, $pH = 7$, $C_0 = 8$ mg/L, $T = 25^\circ C$).

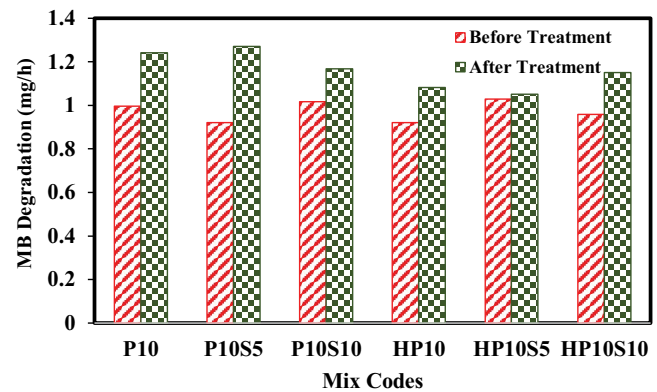


Fig. 9. Degradation rate of methylene blue before and after acid treatment ($Q = 12$ L/min, $pH = 7$, $C_0 = 12$ mg/L, $T = 25^\circ C$).

Among these results, acid treatment had the most significant effect on the performance of the P10S10 specimen. In addition, the lowest impact on the HP10S5 specimen was that the high abrasion resistance of this specimen and its ideal density could be considered the logical reasons for this slight increase. At this concentration, the degradation rate also reaches 0.800 mg/h.

Furthermore, the P10S10 specimen has the highest efficiency after acid treatment. In this category of initial concentration, all normal specimens have higher efficiency, and acid treatment has the most significant effect on them than high-performance specimens. The least impact of acid treatment is seen on the HP10S5 specimen, repeated in the new concentration, similar to the previous figure. The higher performance and consequently higher MB degradation rate at higher concentrations of the pollutant can be attributed to the higher impact quantity of water-soluble pollutant molecules on the photocatalytic surface. As a result, with the reduction of the pollutant concentration, the number of impacts and the amount of the photocatalytic reaction will decrease, which leads to a lower rate of MB degradation [28]. The relatively small difference of the specimens in the degradation rate, especially after acid treatment, can be seen in Fig. 9, except that the P10S5 specimen has the record of the highest degradation rate and the highest increase in the efficiency due to acid treatment with 37.97%.

Based on Fig. 10, the increase in yield due to the increase in initial concentration in different specimens is obtained based on the data reported in Figs. 7–9. This growth rate in output obtained in mg of initial concentration is the highest before and after acid treatment for P10S10 and P10S5 at 0.09 and 0.11 mg/h-mgT, respectively. In addition, the most significant effect of acid treatment on this rate is seen in the P10S5 specimen, with a 42.1% increase. Due to the necessity for acid treatment to reactivate the composite surface, these results mean that the P10S5 specimen shows the best potential at high concentrations and owns maximum photocatalytic activity, among other specimens.

3.4. Effect of initial pH

According to Fig. 11, the alkaline/acid concentration variations in pH 3–11 did not lead to significant changes in the degradation rate of MB, and the sensitivity of the output to pH variations is low. So, this technology can be used in wastewater environments, especially in textile industries.

3.5. Reusability of photocatalytic cement composites

The reusability of fabricated composites is considered by the cost and the ability of the surface activation, which is one of the important parameters in photocatalytic purification [42]. After testing the specimens for the first time, the same specimens were subjected to the acid-treatment process. This process restored the activity of the surface completely and even increased the performance of the PCCs (Figs 7–9).

3.6. Mechanism of MB photocatalytic degradation

Fig. 12 demonstrates the possible mechanism of MB degradation on the photocatalytic cement composite surface. Initially, the electrons (e^-) in the energy band of TiO_2 move to a higher energy level, leaving holes (h^+) in the valence band. These electrons can transfer energy and reduce O_2 molecules in the solution to $\text{O}_2^{\cdot-}$. In the next phase, $\text{O}_2^{\cdot-}$ reacts with h^+ in water and produces HO_2^{\cdot} .

HO_2^{\cdot} reacts with e^- and h^+ to produce H_2O_2 , and H_2O_2 is reduced to OH^{\cdot} . Alternatively, holes can oxidize OH^- in

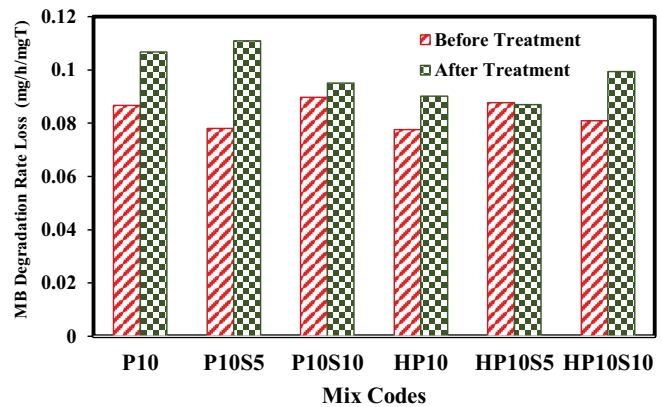


Fig. 10. Decrease in methylene blue degradation rate based on initial concentration before and after acid treatment ($Q = 12$ L/min, $\text{pH} = 7$, $T = 25^\circ\text{C}$).

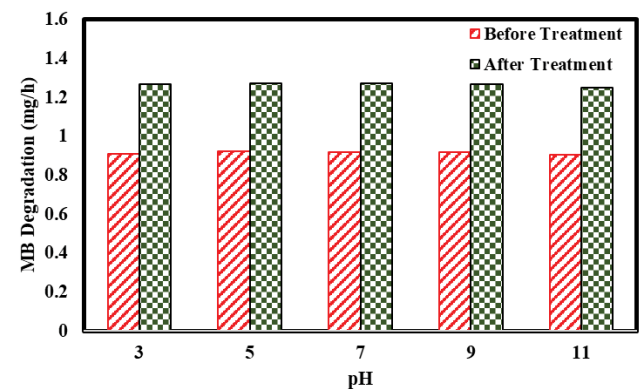


Fig. 11. Changes in methylene blue degradation rate in environments with different pH ($Q = 12$ L/min, $C_0 = 12$ mg/L, $T = 25^\circ\text{C}$).

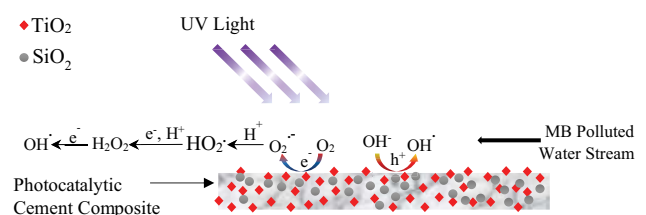


Fig. 12. Schematic description of methylene blue degradation on P10S5 substrate under UV radiation.

water to form OH^{\cdot} . These active species have a very high reduction ability and degrade organic molecules into smaller molecules such as CO_2 , H_2O , etc. [43]. In photocatalytic cement composite substrates, a trivial amount of permeability exists, which mainly leads to the saturation of surface cavities hidden from direct UV radiation and far away from the energy of polluted water flow [44]. Unlike impermeable substrates, the surface absorption in the PCC has a negligible effect on the efficiency. As a vantage point, the acid treatment process intensifies the photocatalytic reaction.

Table 4
Mechanical properties of PCC specimens

Mix code	Strength class	Silica fume content (% wt. of binder) ^a	Compressive strength (MPa)	Flexural strength (MPa)	Abrasion loss (%W)	ALR (%) ^b	ALR (%) ^c
P10	N	0	48.6	5.1	0.31	0	0
P10S5	N	5	51.8	5.4	0.2	35.5	35.5
P10S10	N	10	54.3	6.2	0.17	45.2	45.2
HP10	HP	0	78.8	8.6	0.22	0	29
HP10S5	HP	5	93.1	9.7	0.14	36.4	54.8
HP10S10	HP	10	95.2	10.9	0.11	50	64.5

^aBinder = Cement + Silica fume + TiO₂ (Table 2);

^bALR is calculated separately for each strength class;

^cALR is calculated compared to P10.

3.7. Comparison of the results with literature

Table 5 shows a comparison between the results of different studies. Although there are very high removal rates in different reactors, these points are the initial volume, the energy, the time spent for purification, and subsequently, the energy required to purify a specific amount of pollutant and the efficiency of the photocatalytic surface (purification rate per surface unit). Therefore, only considering the removal rate as a criterion for comparison is not logical, and reactor parameters should be included in the calculations as much as possible. Based on the calculations made according to Eqs. (1)–(4), very high removal efficiency of up to 95% has also been reported in Feng et al.'s research, while the removal efficiency of the current study reactor in the P10S5 design after acid treatment reaches a maximum of 45%. At first glance, this efficiency may indicate the failure of the experiment. However, considering the initial volume of polluted water and the power of the UV source, it is easy to recognize that there is higher efficiency in terms of energy consumption and photocatalytic capability of the surface. Such that the energy consumption of other studies to remove the same amount of pollutant is more than 100 times that of the reactor of this study, and the photocatalytic efficiency of the fixed-bed of the present reactor is at least 67% higher than the best of previous results [44]. Considering these important parameters, unlike other research, the TiO₂ used is not in the nano range and is an industrial grade. In addition, due to its uniform distribution in the depth of the PCC, the performance of the TiO₂ used will continue even due to deep erosions, and its pollution in case of erosion will be far less due to the absence of resins and nanomaterials.

$$KT = \ln \frac{C_0}{C_T} \quad (1)$$

$$RE = (C_0 - C_T) \times \frac{100}{C_0} \quad (2)$$

$$MRE = \frac{PT}{(VC_0 \times RE)} \quad (3)$$

$$SRE = \frac{(VC_0 \times RE)}{(T \times A)} \quad (4)$$

where K is the reaction constant, T is the total treatment time, C_0 is the initial molar concentration of the solution, C_T is the molar concentration at the end of the treatment time, RE is the pollutant removal efficiency during the treatment period, MRE is the energy required to remove one mole of the pollutant, P is the power of the UV source in kW, V is the initial volume of polluted water in liters, SRE is the pollutant removal rate per unit photocatalytic surface, and A is the total photocatalytic surface exposed to UV radiation.

4. Conclusions

In this study, based on the data obtained from various spectroscopic tests of methylene blue contaminated water during a series of experiments, the results were inferred, which could be summarized as follows:

- The study of the microstructure of the P10S5 specimen showed that acid treatment led to the creation of pores less than 200 nm in size on the surface of the specimens, and EDS analysis also showed a high concentration of TiO₂ particles on the surface of the specimen after acid treatment. This high porosity, on the one hand, by increasing the contact surface with polluted water, and on the other hand, by activating the higher number of TiO₂ particles on the surface, leading to a significant increase in the degradation rate.
- Increasing the initial concentration of MB led to an increase in the rate of degradation in the fixed-bed photoreactor, which stood for all specimens in both the intact and acid-treated states. It was found that the designed system and the photocatalytic cement composites in higher concentrations are more efficient.
- It was found that acid treatment significantly increases the efficiency of photocatalytic activity of cement composites in such a way that with an increase of 42.1% in the degradation rate compared to the intact state, the maximum degradation rate is 1.27 mg/h with an initial concentration of 12 mg/L. Obtained by acid-treated P10S5 specimen.

Table 5
Comparison of the degradation rates of methylene blue obtained by several studies and the current study in terms of removal efficiency, reaction rate constant, molar removal energy, and surface removal rate

Photocatalyst/ Support	TiO ₂ particle size (nm)	Volume of MB sol. (mL)	[MB] ₀	Power (W)	Contact surface (cm ²)	Irradiance (mW/cm ²)	Time (min)	K (min ⁻¹)	Removal effi- ciency (%)	Molar removal energy (kWh/mol)	Surface removal rate (×10 ⁻¹⁰ mol/ min·cm ²)	References
TiO ₂ -Glass	11–31 (P25)	3	3.00E-05	0.9	9	100	60	2.2	94	10.6	15.67	[47]
TiO ₂ -Quartz	11–31 (P25)	5	1.20E-06	1.44	71.8	20	300	0.001	62	1,935.5	0.02	[35]
TiO ₂ -Glass	11–31 (P25)	3	3.00E-05	16	14545	1.1	60	–	65	273.5	0.01	[48]
TiO ₂ -WE	11–31 (P25)	50	3.10E-05	300	78.5	3822	50	–	95	169.8	37.52	[44]
TiO ₂ -CC (P1055)	200–300 (KA100)	5,000	3.75E-05	24	361	66.5	240	0.001	29	1.8	62.76	This study
TiO ₂ -CC (P1055A)	200–300 (KA100)	5,000	3.75E-05	24	361	66.5	240	0.002	45	1.1	97.39	This study

- Specimens made with high-performance cement composites obtained a lower degradation rate, but due to greater abrasion resistance, their weight loss due to erosion with water flow is less. Therefore, in long-term operations, it leads to the extended service life of the part. In addition, less mass loss during the acid treatment process will occur.
- pH variations in the range of 3–11 did not significantly affect the photocatalytic performance of the reactor in MB degradation, demonstrating the reactor's performance stability in acidic and alkaline polluted waters.
- Based on the definitions of pollutant removal efficiency that existed so far and according to the scale of the tests, new comparison terms were defined. Considering the initial volume of polluted water, the power consumption of the UV source and the degradation rate, it can be stated that the system tested in this study without using nanomaterials and high power sources can degrade higher amounts of MB compared to other studies.

Acknowledgments

The authors express their gratitude to colleagues from the Academic Center for Education, Culture and Research environmental research institute.

Grant support details

The present research did not receive any financial support.

Conflict of interests

The authors declare that there is no conflict of interest regarding the publication of this manuscript. In addition, the authors observed ethical issues, including plagiarism, informed consent, misconduct, data fabrication and/or falsification, double publication and submission, and redundancy.

Life science reporting

No life science threat was practiced in this research

References

- [1] S. Baruah, N.M. Khan, J. Dutta, Perspectives and applications of nanotechnology in water treatment, *Environ. Chem. Lett.*, 14 (2016) 1–14.
- [2] S.-Y. Lee, S.-J. Park, TiO₂ photocatalyst for water treatment applications, *J. Ind. Eng. Chem.*, 19 (2013) 1761–1769.
- [3] H. Alalwan, A. Alminshid, An in-situ DRIFTS study of acetone adsorption mechanism on TiO₂ nanoparticles, *Spectrochim. Acta, Part A*, 229 (2020) 117990, doi: 10.1016/j.saa.2019.117990.
- [4] Q. Guo, C. Zhou, Z. Ma, X. Yang, Fundamentals of TiO₂ photocatalysis: concepts, mechanisms, and challenges, *Adv. Mater.*, Special Issue: DICP's 70th Anniversary Special Issue on Advanced Materials for Clean Energy, 31 (2019) 1901997, doi: 10.1002/adma.201901997.
- [5] K.P. Gopinath, N.V. Madhav, A. Krishnan, R. Malolan, G. Rangarajan, Present applications of titanium dioxide for the photocatalytic removal of pollutants from water: a review, *J. Environ. Manage.*, 270 (2020) 110906, doi: 10.1016/j.jenvman.2020.110906.

- [6] J.-M. Herrmann, C. Guillard, P. Pichat, Heterogeneous photocatalysis: an emerging technology for water treatment, *Catal. Today*, 17 (1993) 7–20.
- [7] R.F.P. Nogueira, W.F. Jardim, TiO₂-fixed-bed reactor for water decontamination using solar light, *Sol. Energy*, 56 (1996) 471–477.
- [8] I.G. Richardson, The nature of C-S-H in hardened cements, *Cem. Concr. Res.*, 29 (1999) 1131–1147.
- [9] A. Korpa, T. Kowald, R. Trettin, Hydration behaviour, structure and morphology of hydration phases in advanced cement-based systems containing micro and nanoscale pozzolanic additives, *Cem. Concr. Res.*, 38 (2008) 955–962.
- [10] G. Li, Properties of high-volume fly ash concrete incorporating nano-SiO₂, *Cem. Concr. Res.*, 34 (2004) 1043–1049.
- [11] K. Sobolev, M.F. Gutiérrez, How nanotechnology can change the concrete world, *Am. Ceram. Soc. Bull.*, 84 (2005) 16–20.
- [12] J. Vera-Agullo, V. Chozas-Ligero, D. Portillo-Rico, M.J. García-Casas, A. Gutiérrez-Martínez, J.M. Mieres-Royo, J. Grávalos-Moreno, Mortar and Concrete Reinforced With Nanomaterials, Z. Bittnar, P.J.M. Bartos, J. Němeček, V. Šmilauer, J. Zeman, Eds., *Nanotechnology in Construction 3*, Springer, Berlin, Heidelberg, 2009, pp. 383–388.
- [13] A. Nazari, S. Riahi, S. Riahi, S.F. Shamekhi, A. Khademno, Assessment of the effects of the cement paste composite in presence TiO₂ nanoparticles, *J. Am. Sci.*, 6 (2010) 43–46.
- [14] A. Karimipour, M. Ghalehnovi, J. de Brito, Effect of micro polypropylene fibres and nano TiO₂ on the fresh- and hardened-state properties of geopolymer concrete, *Constr. Build. Mater.*, 300 (2021) 124239, doi: 10.1016/j.conbuildmat.2021.124239.
- [15] B.Y. Lee, J.J. Thomas, Influence of TiO₂ Nanoparticles on Early C3S Hydration, *Nanotechnology of Concrete: The Next Big Thing is Small*, ACI Convention, New Orleans, LA, USA, 2009, pp. 35–44.
- [16] B.Y. Lee, K.E. Kurtis, Proposed acceleratory effect of TiO₂ nanoparticles on belite hydration: preliminary results, *J. Am. Ceram. Soc.*, 95 (2012) 365–368.
- [17] L. Cassar, Photocatalysis of cementitious materials: clean buildings and clean air, *MRS Bull.*, 29 (2004) 328–331.
- [18] M. Maury-Ramirez, K. Demeestere, N. De Belie, Photocatalytic activity of titanium dioxide nanoparticle coatings applied on autoclaved aerated concrete: effect of weathering on coating physical characteristics and gaseous toluene removal, *J. Hazard. Mater.*, 211–212 (2012) 218–225.
- [19] A. Kumar, M. Khan, J. He, I.M.C. Lo, Recent developments and challenges in practical application of visible-light-driven TiO₂-based heterojunctions for PPCP degradation: a critical review, *Water Res.*, 170 (2020) 115356, doi: 10.1016/j.watres.2019.115356.
- [20] L. Zang, W. Macyk, C. Lange, W.F. Maier, C. Antonius, D. Meissner, H. Kisch, Visible-light detoxification and charge generation by transition metal chloride modified titania, *Chem. Eur. J.*, 6 (2000) 379–384.
- [21] H. Kisch, L. Zang, C. Lange, W.F. Maier, C. Antonius, D. Meissner, Modified, amorphous titania—a hybrid semiconductor for detoxification and current generation by visible light, *Angew. Chem. Int. Ed.*, 37 (1998) 3034–3036.
- [22] Z. Zhang, P.A. Maggard, Investigation of photocatalytically-active hydrated forms of amorphous titania, TiO₂·nH₂O, *J. Photochem. Photobiol., A*, 186 (2007) 8–13.
- [23] N.C. Neyt, D.L. Riley, Application of reactor engineering concepts in continuous flow chemistry: a review, *React. Chem. Eng.*, 6 (2021) 1295–1326.
- [24] D. Wang, M.A. Mueses, J.A.C. Márquez, F. Machuca-Martínez, I. Grčić, R.P.M. Moreira, G.L. Puma, Engineering and modeling perspectives on photocatalytic reactors for water treatment, *Water Res.*, 202 (2021) 117421, doi: 10.1016/j.watres.2021.117421.
- [25] M. Pelzer, S.L. Pirard, C.A. Páez, J.C. Monbaliu, B. Heinrichs, Development of a continuous fluidic reactor for the photocatalytic treatment of liquid effluents, *J. Nanotechnol. Mater. Sci.*, 7 (2019) 1–19.
- [26] H.-J. Choi, D.-Y. Yoo, G.-J. Park, J.-J. Park, Photocatalytic high-performance fiber-reinforced cement composites with white Portland cement, titanium dioxide, and surface treated polyethylene fibers, *J. Mater. Res. Technol.*, 15 (2021) 785–800.
- [27] C.M. Ling, A.R. Mohamed, S. Bhatia, Performance of photocatalytic reactors using immobilized TiO₂ film for the degradation of phenol and methylene blue dye present in water stream, *Chemosphere*, 57 (2004) 547–554.
- [28] M. Abbas, M. Trari, Contribution of photocatalysis for the elimination of Methyl Orange (MO) in aqueous medium using TiO₂ catalyst, optimization of the parameters and kinetics modeling, *Desal. Water Treat.*, 214 (2021) 413–419.
- [29] Z. Li, X. Chen, M. Wang, X. Zhang, L. Liao, T. Fang, B. Li, Photocatalytic degradation of Congo red by using the Cu₂O/α-Fe₂O₃ composite catalyst, *Desal. Water Treat.*, 215 (2021) 222–231.
- [30] N.M. Mahmoodi, M. Arami, N.Y. Limaee, N.S. Tabrizi, Kinetics of heterogeneous photocatalytic degradation of reactive dyes in an immobilized TiO₂ photocatalytic reactor, *J. Colloid Interface Sci.*, 295 (2006) 159–164.
- [31] R.A. Damodar, T. Swaminathan, Performance evaluation of a continuous flow immobilized rotating tube photocatalytic reactor (IRTPR) immobilized with TiO₂ catalyst for azo dye degradation, *Chem. Eng. J.*, 144 (2008) 59–66.
- [32] S. Mozia, M. Tomaszewska, A.W. Morawski, Photodegradation of azo dye Acid Red 18 in a quartz labyrinth flow reactor with immobilized TiO₂ bed, *Dyes Pigm.*, 75 (2007) 60–66.
- [33] A.R. Khataee, A.R. Amani-Ghadim, M. Rastegar Farajzade, O. Valinzhad Ourang, Photocatalytic activity of nano-structured TiO₂-modified white cement, *J. Exp. Nanosci.*, 6 (2011) 138–148.
- [34] S. Feng, J. Song, F. Li, X. Fu, H. Guo, J. Zhu, Q. Zeng, X. Peng, X. Wang, Y. Ouyang, F. Li, Photocatalytic properties, mechanical strength and durability of TiO₂/cement composites prepared by a spraying method for removal of organic pollutants, *Chemosphere*, 254 (2020) 126813, doi: 10.1016/j.chemosphere.2020.126813.
- [35] K. Natarajan, T.S. Natarajan, H.C. Bajaj, R.J. Tayade, Photocatalytic reactor based on UV-LED/TiO₂ coated quartz tube for degradation of dyes, *Chem. Eng. J.*, 178 (2011) 40–49.
- [36] ASTM International, C150, Standard Specification for Portland Cement, 2005.
- [37] ASTM International, C1240, Standard Specification for Silica Fume Used in Cementitious Mixtures, 2020.
- [38] ASTM International, C494/C494M, Standard Specification for Chemical Admixtures for Concrete, 2019.
- [39] ASTM International, C109/C109M, Standard Test Method for Compressive Strength of Hydraulic Cement Mortars (Using 2-in. or [50-mm] Cube Specimens), 2013.
- [40] ASTM International, C348, Standard Test Method for Flexural Strength of Hydraulic-Cement Mortars, 2021.
- [41] ASTM International, C944/C944M, Standard Test Method for Abrasion Resistance of Concrete or Mortar Surfaces by the Rotating-Cutter Method, 2019.
- [42] A. Mohagheghian, S.-A. Karimi, J.-K. Yang, M. Shirzad-Siboni, Photocatalytic degradation of a textile dye by illuminated tungsten oxide nanopowder, *J. Adv. Oxid. Technol.*, 18 (2015) 61–68.
- [43] L. Lu, R. Shan, Y. Shi, S. Wang, H. Yuan, A novel TiO₂/biochar composite catalysts for photocatalytic degradation of methyl orange, *Chemosphere*, 222 (2019) 391–398.
- [44] S. Feng, F. Liu, X. Fu, X. Peng, J. Zhu, Q. Zeng, J. Song, Photocatalytic performances and durability of TiO₂/cement composites prepared by a smear method for organic wastewater degradation, *Ceram. Int.*, 45 (2019) 23061–23069.
- [45] H. Anwer, A. Mahmood, J. Lee, K.-H. Kim, J.-W. Park, A.C.K. Yip, Photocatalysts for degradation of dyes in industrial effluents: opportunities and challenges, *Nano Res.*, 12 (2019) 955–972.
- [46] D.S. de Sá, L.E. Vasconcellos, J.R. de Souza, B.A. Marinkovic, T. Del Rosso, D. Fulvio, D. Maza, A. Massi, O. Pandoli, Intensification of photocatalytic degradation of organic

- dyes and phenol by scale-up and numbering-up of meso- and microfluidic TiO₂ reactors for wastewater treatment, *J. Photochem. Photobiol., A*, 364 (2018) 59–75.
- [47] L. Lei, N. Wang, X.M. Zhang, Q. Tai, D.P. Tsai, H.L.W. Chan, Optofluidic planar reactors for photocatalytic water treatment using solar energy, *Biomicrofluidics*, 4 (2010) 043004, doi: 10.1063/1.3491471.
- [48] N. Wang, L. Lei, X.M. Zhang, Y.H. Tsang, Y. Chen, H.L.W. Chan, A comparative study of preparation methods of nanoporous TiO₂ films for microfluidic photocatalysis, *Microelectron. Eng.*, 88 (2011) 2797–2799.